

RESEARCH ARTICLE

Petrogenetic of Igneous Complex of Iloa Nanasi Gold Deposit, Gunung Pani, Gorontalo, Indonesia

Iryanto Rompo^{1,*}, Fajar Ismail², STJ Budi Santoso³, Mega Fatimah Rosana⁴, Euis Tintin Yuningsih⁴

¹ PT J Resources Nusantara, Equity Tower, SCBD, Jl. Jend Sudirman, Jakarta - 12190, Indonesia

² PT Gorontalo Sejahtera Mining, Desa Hulawa, Kec. Buntulia, Pohuwato, Gorontalo – 96266, Indonesia

³ PT Geofix Indonesia, Amaryllis Townhouse Kemang, Jl. Bangka XIA No.5, Jakarta – 12720, Indonesia

⁴ Geology Engineering, Padjadjaran University, Jl. Raya Bandung – Sumedang Km. 12, Jatinangor - 45363, Indonesia

* Corresponding author : ahmad.rompo@jresources.com

Tel: +62-811-1555-665

Received: Aug 26, 2023; Accepted: Dec 6, 2023.

DOI: 10.25299/jgeet.2023.8.4.14250

Abstract

Iloa Nanasi Au-Ag deposit located in the western flank of the Gn. Baganite, a part rhyodacite dome in Gn. Pani district, Gorontalo Province, where the extensive exploration programs were carried out by PT Gorontalo Sejahtera Mining (a subsidiary of PT J Resources Nusantara) from 2012 – 2020. As the result, a total of 72.7 Mt @ 0.98 g/t Au and 0.85 g/t Ag (2.3 Moz Au and 2.6 Moz Ag) mineral resource was delineated in 2019. This paper mainly aimed to the petrogenesis association of granitoid basement and rhyodacite unit as the host rock in the Iloa Nanasi gold deposit.

The geology of Iloa Nanasi is overlain by Late Miocene granodiorite, andesite and diorite basement, Pliocene volcanic complex predominantly dacite – rhyodacite, tuff, breccia, and quaternary deposit as alluvial and surface breccia. Hydrothermal alteration and gold – silver mineralization centered in the porphyritic rhyodacite host rocks where the intense silicification forming a zone around the hydrothermal crackle breccia unit and/or high-density quartz vein, veinlets and stockworks. Mineralization in Iloa Nanasi is interpreted as a low sulfidation epithermal system dominated by a large volume of hydrothermal crackle breccia, intense quartz veining, veinlets, and high-density fracturing.

A combined analytical result of petrography and whole-rock geochemistry has been used to assess the petrogenetic association of the rhyodacite and granitoid basement in the Iloa Nanasi. The result of the AFM diagram plot shows sample trends in calc-alkaline magma field. In contrast, the SiO₂ – K₂O plot distributed in two trends: the older unit was associated with high-K calc-alkaline and the shoshonite series for the younger unit. The changing of magma series is considered as product of crystallization differentiation of evolved parental magma or derived from the melting of mantle material after the mantle or lower crustal was metasomatized during a former episode of subduction.

Keywords: petrogenesis, petrology, tectonic, alteration, mineralization, epithermal, Gn. Pani, Iloa Nanasi

1. Introduction

The Iloa Nanasi gold prospect is situated in the western flank of Gn. Baganite, part of Gn. Pani district, with estimated mineral resource 72.74 Mt @ 0.98 g/t Au and 0.85 g/t Ag (Pratama and Wijayadi, 2020). The mineral prospect is lies within 5th Generation Contract of Work (CoW) Pani Block granted to PT Gorontalo Sejahtera Mining (GSM) in the Regency of Pohuwato, Province of Gorontalo, Indonesia. This area is approximately 120 km westward of the provincial capital Gorontalo, or 15 km north of the main town Marisa, the capital of the Pohuwato regency. The CoW block encompasses an area of 7,385 ha. It contains several gold prospects of epithermal mineralization hosted in the Pliocene rhyodacite dome complex, Gn. Pani district e.g., Iloa Nanasi, Pani Ridge, Kolokoa, Lone Pine, Borose, Masina, Ponelo, Wadi, Jahiya, and Iloa Bawah (McConnochie, 1999; Rompo and Santoso, 2019).

The early exploration of gold in Gn. Pani district started since Dutch era and mainly focused on the Pani Ridge prospect by previous explorers e.g., Tropic Endeavour, BHP, One Asia, Newcrest, Avocet Mining Plc., J Resources Nusantara. In 2022 the project was acquired by Merdeka Copper Gold and fully controlled the exploration activity in Gn. Pani district. Although the exploration data resulting from extensive exploration produces significant geological information, this paper only dedicated to the petrological characteristics and petrogenesis

association of the granitoid basement and rhyodacite as the primary host of gold mineralization in Iloa Nanasi. The data obtained in this paper compiled from geological mapping, geochemical data, drilling, core logging and others supported laboratory analysis e.g., petrography and whole-rock analysis.

2. Literature Review

2.1 Previous Work

Gn. Pani district has been explored since the Dutch era, e.g., van Schelle (1889) investigate some of the gold deposits in North Sulawesi and Gorontalo and then followed by operation of four underground mines between 1896 – 1929 including the construction of exploration tunnel by “Exploratie Syndicaat Pagueat” in Gn. Pani and two attempts to mine Gn. Pani between 1908 – 1910 (Koperberg, 1929; McLellan et al., 1975; van Leeuwen and Pieters, 2011).

The first geological information of Gn. Pani and the surrounding area was provided by Trail et al. (1974) interpreted the Pani Volcanics to be widespread in the Marisa hinterland and occurred as ridge-top capping of higher elevation terrain. It is mixed with older intrusive and metamorphic rocks and the name of Bumbulan Granodiorite Complex was applied for intrusive rock. Following the exploration by Tropic Endeavour Indonesia (TEI), McLellan et al. (1975) identify gold mineralization in Gn. Pani associated with the dacitic flows, agglomerates, tuffs, with subordinate rhyolite and

andesite members. Whittle (1975) noted two stages of silicification: an initial deuteric silicification accompanied by sericitization, and second stage associated with potassic metasomatism and pyrite.

Kavalieris et al. (1982) established a lithological unit in Gn. Pani with general term “Pani-type igneous rocks”, composed of porphyritic rhyodacite, rhyodacitic volcanic, rhyodacitic lapilli tuff, rhyodacite, and porphyritic micro-granodiorites. The porphyritic rhyodacite is highly silicified and accompanied by complete sericitization after the biotite phenocrysts, pervasive sericitization of the matrix and replacement of plagioclase phenocryst by sericite, calcite, and quartz veining. A further study by Kavalieris et al. (1990) concluded that gold mineralization in Pani centered in Gn. Baganite dome complex where the chlorite formation temperature varies from 125-275°, homogenization temperature 150-300° from secondary fluid inclusion of quartz phenocryst. The salinity of most fluid inclusions ranges from near zero up to 4 eq.wt percent NaCl with some elevated as high as 40 eq.wt percent (Kavalieris et al., 1990).

Marjoribanks (1998) in his unpublished report to Newcrest has done a photo-geology interpretation map at 1 : 20,000 scale, divided three main intrusion phases in Pani Volcanic Complex named early Pani intrusive phase P1, main Pani intrusive phase P2, and late Pani intrusive phase P3. According to Marjoribanks (1998) gold mineralization in Pani was introduced during the late stage of P2 into WNW-trending extensional zones along the north and south margin of the P2 complex.

2.2 Regional Tectonic and Geology

Iloa Nanasi gold prospect located in the fertile North Arm of Sulawesi has resulted from the various ‘tectonic interactions’ of three tectonic plates to produce an unusual K-shaped island (see Fig 1). It consists of pre-Tertiary basement of plutonic-

metamorphic complex, and from Eocene to Recent age, comprises marine to subaerial volcanoclastic rock units that younger toward the east with a series of active volcanos at the eastern tip (Sukamto, 1975; Katili, 1978, Hamilton, 1979; Silver et al., 1983; Carlile et al., 1990; Kavalieris et al., 1992; Bachri et al., 1993; Apandi and Bachri, 1997; Effendi and Bawono, 1997; Person and Cairra 1999; Hall., 2002, Kadarusman, 2011; Priadi, 2011; Maulana et al., 2019).

The oldest rocks unit in the North Arm of Sulawesi mainly occurred in the western part from Tolitoli and extend eastward to Pani, comprised of a metamorphic basement and Paleogene Tinombo Formation (Trail et al., 1974; Sukamto, 1973; Ratman, 1976; Kavalieris et al., 1982; Kavalieris et al., 1990; Carlile et al., 1990; Bachri et al., 1993; Maulana et al., 2019). The Tinombo Formation intruded by a series of Oligocene to Miocene granodiorite to monzonite e.g., in Palu has been dated 31 Ma (Sukamto, 1973), Pani dated 17.7 - 12.6 Ma and Gorontalo dated 16.0 Ma (Pearson and Cairra, 1999), and at Tolitoli has been dated 8.2 ± 0.2 to 7.2 ± 0.1 Ma (Maulana et al., 2016; Zhang et al., 2020). Most of these granitoid rocks along the North Arm of Sulawesi are grouped into magnetite series that show more intense mineralisation than the ilmenite-series rocks commonly in the southern part of the island as reported by Maulana et al. (2013).

In the Marisa region where Gn. Pani deposit is located, the Tinombo Formation is unconformably overlain by Pliocene Pani Volcanic Complex that interpreted as eroded volcanic center comprises of pyroclastic, breccias, and massive or flow-banded porphyritic rhyodacites. The volcanic center intruded by hornblende and hornblende-biotite granodiorite that correlated with Pani Volcanics (Kavalieris et al., 1990) and other granitoids e.g., granite, dacite and quartz monzonite that mapped as Bumbubulan Granodiorite by Bachri et al. (1993).

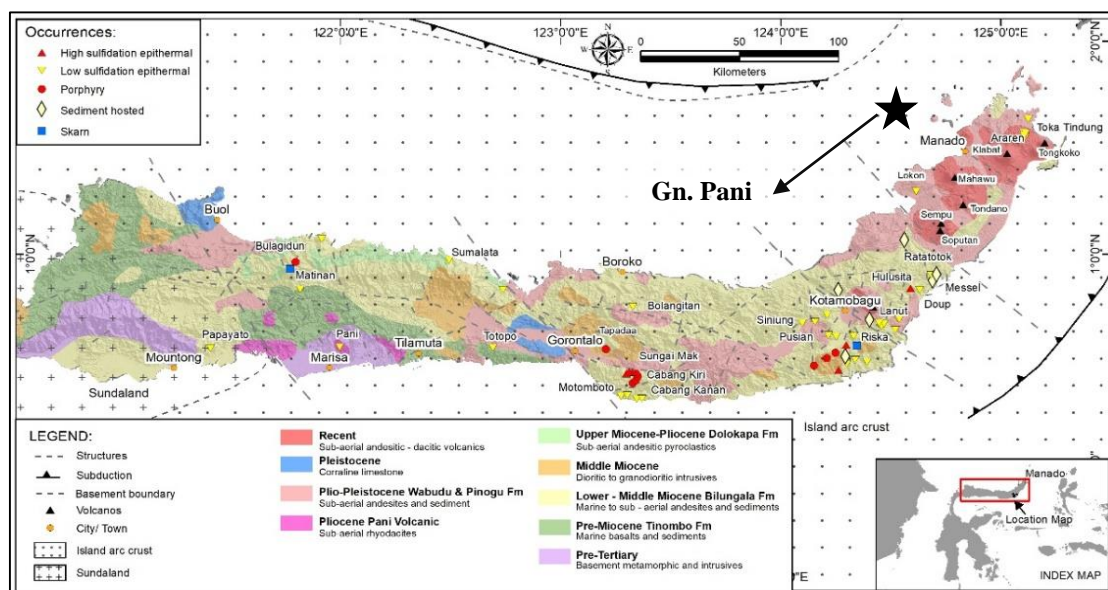


Fig. 1. Regional geology and mineral occurrences along the North Arm Sulawesi (modified after Carlile et al., 1990; Bachri et al., 1993; Apandi and Bachri, 1997; Effendi and Bawono, 1997; Cairra and Pearson, 1999)

2.3 Local Geology

The local geology of the Iloa Nanasi gold deposit comprises of a series of volcanic units interpreted as part of rhyodacitic domes. The oldest igneous rock in the local scale is granodiorite was mapped in Lone Pine (3 km north of Iloa Nanasi) and Simpang Tiga (2 km southwest of Iloa Nanasi).

This unit is intruded by a series of rhyodacitic units that display three distinctive textures e.g., equigranular rhyodacite, porphyritic rhyodacite, and late rhyodacite with include narrow zona of phreatomagmatic breccia and pyroclastic unit (see Fig 2 and Fig 3).

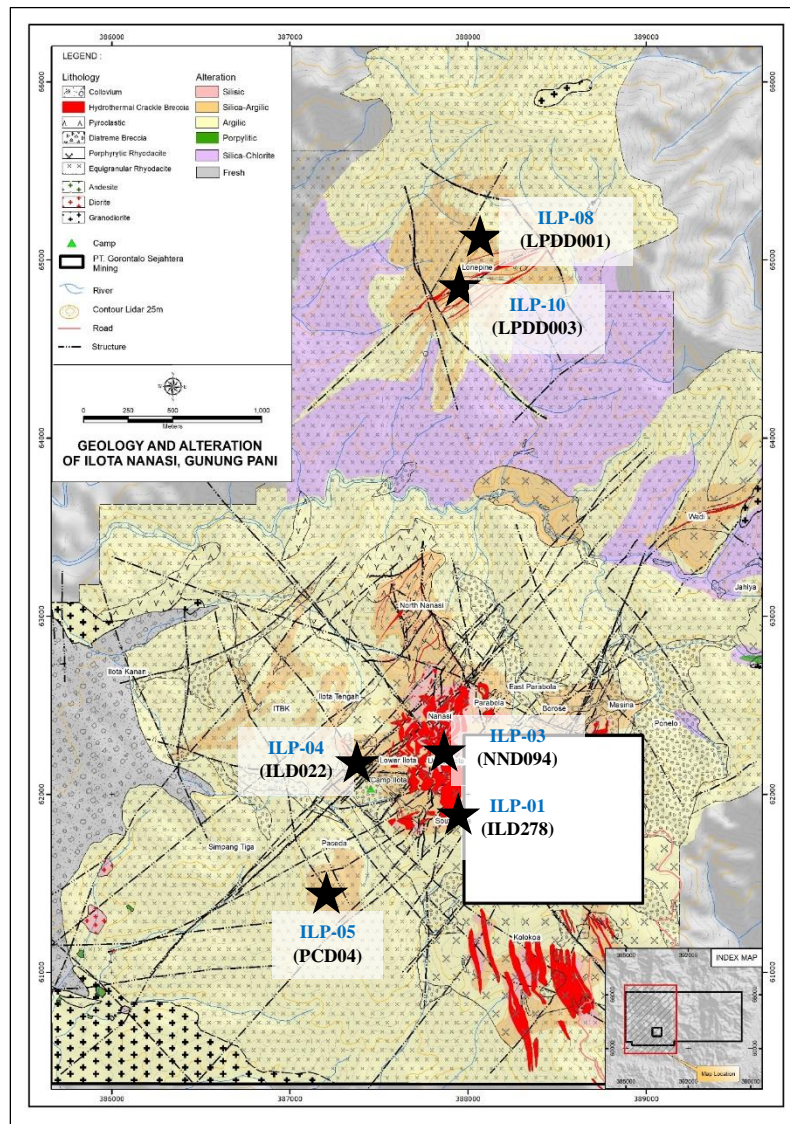


Fig. 2. Local geology, alteration and mineralisation in Iloa Nanasi and showing the distribution of 6 samples examined in this study

Equigranular rhyodacite is distributed in the west margin of Iloa Nanasi characterized by equigranular texture, less than 30% quartz phenocrysts, finer grained, and less altered with the occurrences of well-preserved biotite and hornblende. Toward to the east and center of dome, the rhyodacite unit displays more porphyritic texture and larger quartz phenocrysts that mapped as porphyritic rhyodacite. This unit commonly displays massive to flow-banded structure, quartz phenocryst up to 3 mm, composed by plagioclase, K-feldspar, biotite, albite, and chlorite. This unit is intensely altered and occurred as the host of mineralisation in Iloa Nanasi. The younger rhyodacite intrusion mapped in the Paceda Hill, about 1.0 km southwest of the Iloa Nanasi, display unaltered porphyritic texture.

Phreatomagmatic breccia occurs relatively NE-trending stretching from the Baganite to the Iloa Bawah and South Iloa area and cutting the rhyodacite units. This unit is characterized by mosaic, rotational to chaotic fragments, monomict to polymictic clast, with a slight to wide scale with typically corroded clast texture in the margin of breccia. Whilst the pyroclastic unit e.g., tuff, lapilli tuff, and accretionary lapilli are exposed in the high topography at North Nanasi, Borose Masina Ponelo, Iloa Tengah Bawah Kanan, and Kolokoa. The pyroclastic unit generally shows sub-horizontal bedding, weakly mineralized and less altered than the rhyodacite unit.

Hydrothermal crackle breccia is distributed mainly in the central to the westward of Gn. Baganite and it is thought of as the younger unit in Iloa Nanasi that cuts all the oldest rock units and is spatially associated with gold mineralization. This unit is characterized by monomictic clast, subangular, hydrothermally cemented and contains a sulfide matrix. From the drilling data, these units have a limited vertical extent of about 150 m up to 400 m and dip moderately to steep towards the inferred volcanic center of Gn. Baganite.

All the rock units are covered by locally thin surficial deposits of colluvium. This deposit is the youngest unit, a product of erosion and deposition comprising the lithic fragment of rhyodacite intrusive and lava, breccia clasts, pyroclastic, and crackle breccia fragments.

2.4 Structure

The NE corridor of regional structure is the main control of mineralization at Iloa Nanasi where the mineralisation is developed in a multi-direction of open-space filling structures within NE corridor.

The pre- and syn-mineralization structures interpreted as the structures control the hypogene mineralization and generated stockworks and vein zones (crackle breccia) that controlled by the conjugate structures within NE corridor of the regional structures. The pre- and syn-mineralization structure

also can be tracked from the individual zone of crackle breccia that corresponding the mineralization zone that generally has NNE to NE direction with minor NW and NS extension.

The post and late structures are the latest structures and/or reactivated structures that parallel, cut and/or displaced the mineralization in Iloa Nanasi. The post and reactivated structures also control the oxidation zone and the supergene mineralization. The major structural orientations mapped are oriented NE/SW and NW – WNW with sub-vertical dip (possibly dip-slip). These structures are nested in a W-NW Miocene basement corridor and consistent with W-NW striking dextral strike slip faulting. The NE/SW structures with sub-vertical dip slip are consistent with extension within a W-NW striking dextral strike slip fault system. The volcanic architecture of the Pani dome has been defined by mapping of flow banding in the rhyodacite lava flows which generally dip inwards towards Gn. Baganite.

5.3 Hydrothermal Alteration and Mineralization

Hydrothermal alteration in Iloa Nanasi generally developed well surrounding the hydrothermal crackle breccia and/or veining and affected the rocks around resulting in the mineralogical and geochemical zonation pattern. The alteration mineral zonation reconstruction around the Iloa Nanasi was done by combining of the drill core logging, petrography, and short-wave infrared (SWIR) reflectance spectroscopy method. A total of 19 samples were tested for petrography, meanwhile the SWIR work was carried out using TerraSpec analyzer for 98 holes in 12 constructed sections (Szentpeteri 2017, 2019; Rura and Siburian, 2019).

The surface alteration of Iloa Nanasi is represented by intense silicification to the center of mineralization and occupied a large area. The silicification is graded distally to argillic alteration and further to propylitic alteration. Silicification is defined by pervasive alteration with glassy altered groundmass replaced by mosaic/felsic-textured fine crystalline quartz and K-feldspar. The phenocryst is also partially altered to quartz – albite – chlorite ± adularia and traces of sericite + smectite + halloysite + kaolinite + white mica. Adularia is seemed to present locally and only can be identified during petrography study due to its very fine grain size. A smaller tabular ferromagnesian mineral (probable pyroxene and/or biotite) is completely replaced by quartz – sericite - adularia alteration pseudomorphs and in places containing disseminated sulphides/oxides/hydroxides.

The silicification forms a zone around the hydrothermal breccia unit and /or high-density quartz-veins, veinlets and stockwork. From the geophysical survey, the silica altered rock in Iloa Nanasi is characterized by a high resistivity response based on the ground IPDD survey and low conductivity of airborne electromagnetic. This resistive zone also coincided with a low magnetic respond as the result of magnetic destructive alteration process and forming a zone to the deeper level. The airborne conductivity result is also coincided with the mapped lateral silicification that corresponds to alteration extension to the north of Gn. Baganite. Several soil and drainage sampling results also confirmed the alteration pattern. From soil sampling data, the distribution of Au and Ag has moderate correlation, moreover a patchy distribution occurs in Kolokoa, Borose Masina Poneo, Wadi and Jahiya that associated with the narrow body of mineralized veins.

Toward the distal, intense clay argillic alteration forms an envelope of silicification and consists of various amount of clay e.g., montmorillonite, nontronite, halloysite, illite, phengite, kaolinite and chlorite as observed from the SWIR data (Rura and Siburian, 2019). In addition, chlorite is commonly present and replacing mafic mineral e.g., biotite and partially

plagioclase and sanidine phenocrysts. The presence of chlorite is quite common in all alteration zones in Iloa Nanasi and Pani district in general as observed by Kavalieris et al. (1990).

Gold mineralization in Iloa Nanasi is interpreted as a low sulfidation epithermal system (LSE) based on the presence of adularia and other characteristics e.g., dominant neutral clay alteration, low total sulfide content, base metals, and low silver to gold ratio. The mineralization is dominated by a large volume of hydrothermal crackle breccia, intense quartz veining and veinlets, and high-density fracture that differ from classic low sulfidation epithermal quartz vein system e.g., Pongkor (Basuki et al., 1994) and Kencana (Clark and Gemmel, 2018). The gold mineralisation in Iloa Nanasi is hosted by porphyritic rhyodacite and is interpreted as dipping moderately to east toward the Gn. Baganite. It is likely this east dip is part of the general inwards dip of the porphyritic rhyodacite.

3. Sampling and Analytical Methods

3.1 Sample Selection

Samples for examination and analysis are selected from the drill cores from the drilling program carried out during exploration by PT Gorontalo Sejahtera Mining (J Resources) from 2012 - 2020. All representative samples were selected based on geological models constructed following extensive field mapping and drill core logging. The samples are selected from several key observation parameters including intrusion, alteration, sulfide mineralogy, oxidation, hypogene mineral and supergene iron oxides, veining textures, composition, structures, and fractures.

A total of 6 samples were selected (Fig 02) comprised of 4 samples representing rhyodacite series that were collected from the drill holes in Iloa Nanasi and Paceda e.g., ILP-01 (drillhole ILD278 depth 210m), ILP-03 (drillhole NND094 depth 33.70m), ILP-04 (drillhole ILD022 depth 116.50m), and ILP-05 (drillhole PCD04 depth 60m). The other two samples representing granitoid basement were collected from Lone Pine e.g., ILP-08 (drillhole LPDD001 depth 125.50m) and ILP-10 (drillhole LPDD003 depth 195m). For comparison, 4 historical samples reported by Kavalieris et al. (1990) were also compiled to support analysis and interpretation.

3.2 Petrography and Whole-rock Geochemistry

A total of 6 samples were collected for their major oxide and trace element of whole-rock composition analysis. Each sample was selected to represent various igneous rock types in Iloa Nanasi, and the remainder was retained for a petrographic examination performed in PT Geomineral Sukma Analisis using Bestscope 5062TTR series microscope (Verdiansyah, 2023).

Whole-rock composition analyses were completed in the laboratory of PT Intertek Service Utama, Jakarta, Indonesia. Major oxide analysis, trace and rare earth element compositions were determined by ICP-MS and XRF analyses. Each raw sample with average weight of 2-3 kg was sort and dry at 105°C then crushed under 2 mm. Up to 250 gr of the sample was then split and pulverized to pass 95% < 75 µm mesh. The trace and rare earth element were determined by ICP-OES/MS following lithium borate fusion and four acid total digestion methods. In contrast, an X-ray fluorescence spectrometer determined the major oxide composition on fused disc and pressed powder sample. Loss on ignition (LOI) was calculated from the changes in sample weight before and after heating to 1,000°C. The detailed analysis procedure can be accessed through the company website in <https://www.intertek.com>.

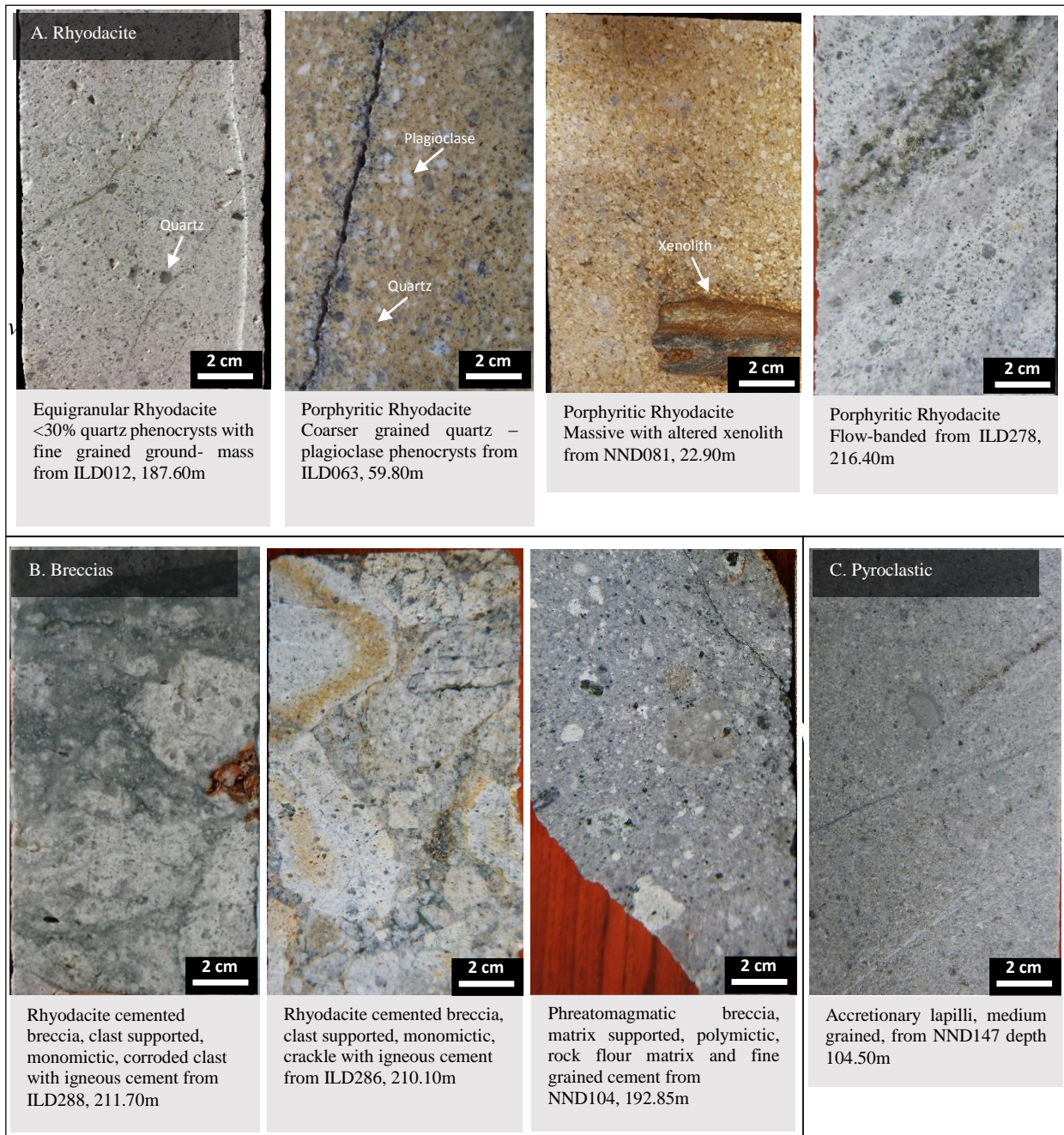


Fig. 3. The local lithological variation of the Iloa Nanasi area shows the general characteristics of the rhyodacite, breccia and pyroclastic rocks

4. Results

The samples examined here were obtained from a total of 6 samples collected from Iloa Nanasi and the surrounding area, as presented in Fig 02, showing each sample location. A total of 6 samples were examined under a microscope and whole-rock analysis, comprised of 4 samples representing rhyodacite series that were collected from the drill holes in Iloa Nanasi and Paceda. e.g., ILP-01, ILP-03, ILP-04, and ILP-05. The other two samples representing granitoid basement were collected from Lone Pine e.g., ILP-08 and ILP-10.

4.1 Igneous Rock Petrography

Based on the visual observation of textures, abundance, and composition of mineral assemblages, the sample of ILP-01 and ILP-03 has been referred to as porphyritic rhyodacite. This unit mainly crops out in the Iloa Nanasi and G. Baganite and mainly hosts gold mineralization. Most of the outcrop has been altered

to silicification and cut by hydrothermal crackle breccia and quartz veins. The field occurrences and photomicrograph of porphyritic rhyodacite are presented in Fig 4A-D.

As observed, the sample of rhyodacite from ILP-01 and ILP-03 showed similar properties of porphyritic texture 25 – 60% of volume, consisting mainly of phenocrysts of quartz, plagioclase, K-feldspar, hornblende, biotite, and minor muscovite. Quartz phenocryst is abundant from 20 – 30% volume of rock and typically coarse grained from 0.7 – 2.0 mm in diameter at ILP-01, whereas sample ILP-03 is typically finer grain and has less phenocryst composition. Plagioclase is euhedral to anhedral, averages 10 – 20% volume of rock, size from 170 – 560 μm composed from andesine to oligoclase and shows various twinning of albite, carlsbad and pericline. In some samples, a microlite is present as well as sanidine. K-feldspar occurred from 15 – 25% volume of rock, typically subhedral with size from 100 μm up to 1.5 mm. Sanidine is

present in less amounts < 10% volume of rock, euhedral to subhedral with size from 100 – 850 μm . Other primary mineral, e.g., biotite present < 10%, hornblende < 5%, and rarely muscovite < 3% volume of rock. Accessories mineral present as zircon and apatite that typically less than 1% volume of rock. In general, both sample of porphyritic rhyodacite are weakly altered where sericite was found replacing biotite, hornblende, or feldspar mineral. Epidote is present in places with chlorite, illite, and smectite.

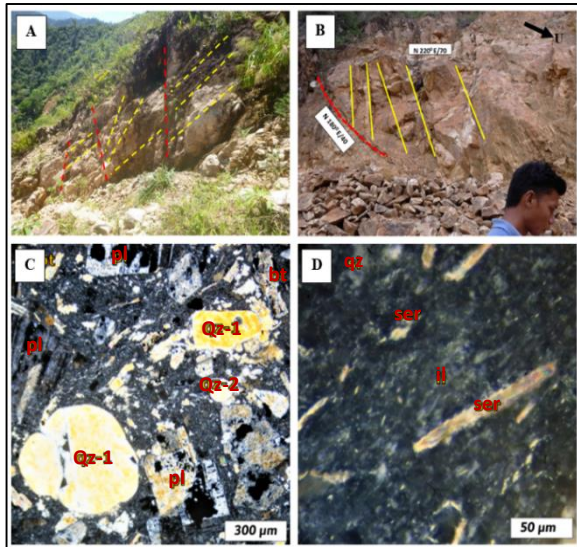


Fig. 4. (A) Outcrop of the porphyritic rhyodacite in Iloa Nanasi showing vertical - sub vertical NNE structure (N 192°E/74°, N 25°E/80°, N 45°E/83) sinistral strike slip fault, and dip slip SW structure (N 255°E/65°, N 234°E/53°) of silica and silica-argillic altered fragmented porphyritic rhyodacite with quartz limonitic rich veinlets; (B) Outcrop of silica altered porphyritic rhyodacite showing vertical fracture on hanging wall zone of NS structure of normal fault (N 180°E/40°); (C) Photomicrograph of porphyritic rhyodacite with up to 60% phenocryst consists of quartz and plagioclase; (D) Sericite replacing microlite in volcanic glass groundmass. (Abbreviation: **il** = illite; **pl** = plagioclase; **qz** = quartz; **ser** = sericite).

A sample of ILP-04 representing less mineralized rhyodacite and mostly fine-grained rhyodacite is presented in Fig 5A-B. Generally, the microscopic properties showed < 25% of phenocryst consists of quartz and K-feldspar set in the volcanic glass groundmass with several altered plagioclase, sanidine, microlite, hornblende, biotite, and apatite. The quartz phenocryst is typically < 20% of volume, fine-grained 0.2 – 0.5 mm, sharp facet, and rim reaction was observed in places. Plagioclase is euhedral to anhedral, averages 10 % volume of rock, has a size from 170 – 560 μm and shows various twinning. K-feldspar has occurred from 10 – 15% volume of rock, typically subhedral with size from 600 - 800 μm , prismatic and weakly altered to sericite. Sanidine is present in less amounts < 10% volume of rock, euhedral to subhedral with sizes from 100 – 850 μm . Other primary mineral, e.g., biotite present < 10% volume of rock, size from 35 – 120 μm , and mostly altered to vermiculite – chlorite – sericite and less muscovite. Hornblende < 5% volume of rock, size from 150 – 450 μm and strongly altered to chlorite – sericite. Accessories mineral present as apatite that typically less than 1% volume of rock, subhedral with 5 – 20 μm in size.

The sample of ILP-05 represents the young rhyodacite that is interpreted as a late intrusion phase in Iloa Nanasi and typically barren is subdivided into alkali feldspar rhyolite. The photomicrograph is presented in Fig 5C – D. Generally, the sample of ILP-05 is coarse-grained, porphyritic texture with an average of 20% in volume. The phenocryst typically has coarse grained quartz and feldspar; and the fine-grained phenocryst

consists of quartz and biotite. Quartz is typically coarse grained from 0.8 – 2.1 mm and has sharp facet. K-feldspar is present from 10 – 15% volume of rock, subhedral crystal with size from 200 – 800 μm , prismatic with carlsbad twinning. Hornblende and biotite are not common, typically less than 5%, euhedral crystal and various sizes where hornblende typically coarse-grained than biotite. Apatite is an accessory mineral with less than 1% volume of rock, subhedral, and size from 5 – 20 μm .

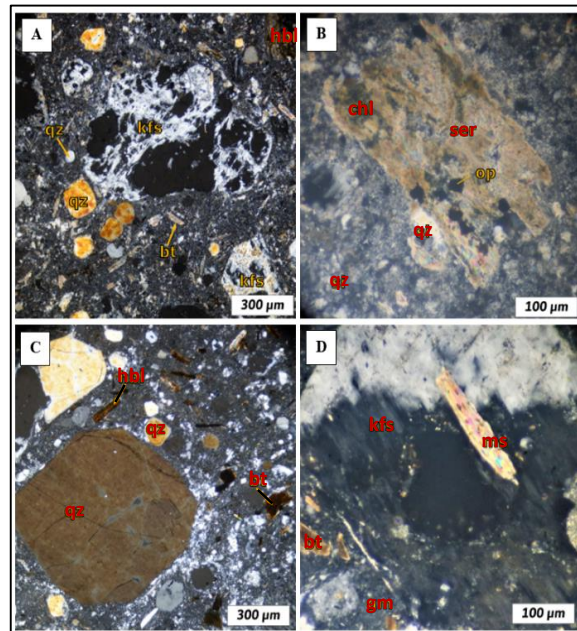


Fig. 5. (A) Sample of equigranular rhyodacite from ILP-04 showing fine-grained quartz phenocrysts; (B) Ragged biotite crystal in sample ILP-04 that has been replaced by sericite and chlorite; (C) Coarse grained quartz crystal of young rhyodacite from ILP-05; (D) Muscovite, biotite, and K-feldspar crystal set in volcanic glass groundmass of sample from ILP-05. (Abbreviation: **bt** = biotite; **chl** = chlorite; **gm** = groundmass; **hbl** = hornblende; **kfs** = K-feldspar; **ms** = muscovite; **op** = opaque; **qz** = quartz; **ser** = sericite).

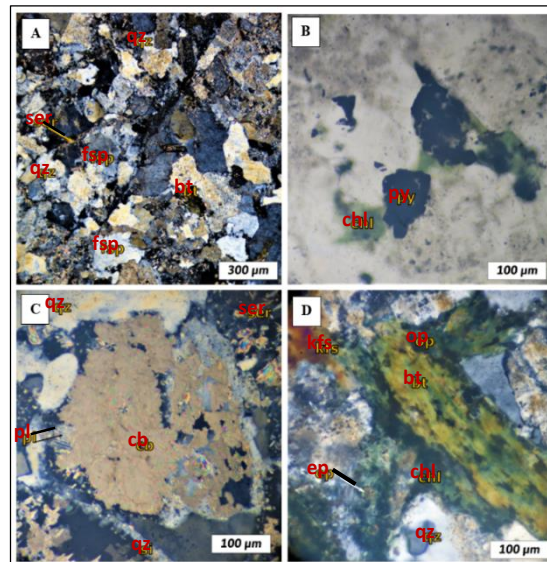


Fig. 6. Photomicrograph of the igneous basement of alkali feldspar granite: (A) Hypidiomorphic and interlocking of quartz, K-feldspar, biotite crystal; (B) Chlorite and pyrite set in groundmass; (C) Calcite and sericite replaced plagioclase and feldspar; (D) Chlorite, epidote and sericite replaced biotite. (Abbreviation: **bt** = biotite; **cb** = carbonate; **chl** = chlorite; **ep** = epidote; **fsp** = feldspar; **kfs** = K-feldspar; **op** = opaque; **pl** = plagioclase; **py** = pyrite; **qz** = quartz; **ser** = sericite).

Sample of ILP-08 and ILP-10 representing the igneous basement that is exposed in the north of Iloa Nanasi and can be subdivided into alkali feldspar granite. The photomicrograph presented in Fig 6A – D. The petrographic properties are show phaneritic, equigranular texture, hypidiomorphic, interlocking, dominant subhedral crystal composition range from 50 μm to 3 mm size consisting of quartz, K-feldspar, plagioclase, biotite, hornblende with some accessories mineral e.g., apatite and tourmaline. Quartz has occurred as an anhedral crystal, disseminated, with an average 35 - 45% volume of rock, size from 100 μm up to 1 mm. K-feldspar is subhedral, prismatic, occupying 30 – 45% volume of rock, size varies from 200 μm to 2.8 mm. Plagioclase is present in 5 – 10% volume of rock, prismatic, subhedral, size from 50 – 500 μm , showing twinning and in part replaced by calcite. Biotite and hornblende are less than 5% volume of rock, tabular to prismatic, size from 100 – 200 μm , and altered to chlorite and sericite. Hematite is found as inclusion in biotite and pyrite observed along the cleavage.

4.2 Whole-rock Geochemistry

Major oxide and trace elements data obtained for the Iloa Nanasi samples and Kavalieris et al. (1990) data were presented in Table 01 and plotted in Fig 07. All rhyodacite samples e.g., ILP-01, ILP-03, ILP-04 and ILP-05 span a short range from 71.63 – 74.39 wt.% SiO_2 and 13.97 – 15.23 wt.% Al_2O_3 , these results are consistent with the previous analysis by Kavalieris et al. (1990). Meanwhile, the granitoid sample was taken in Lone Pine has similar span a short range but slightly lower SiO_2 content from 67.03 – 64.49 wt.% and 14.71 – 14.98 wt.% of Al_2O_3 . The plotting of samples into total alkalis vs silica (TAS) diagram of Le Bas et al. (1986) resulted all the samples from ILP-01, ILP-03, ILP-04, and ILP-05, as well as Kavalieris et al. (1990) data are grouped in rhyolite field (Fig 7A).

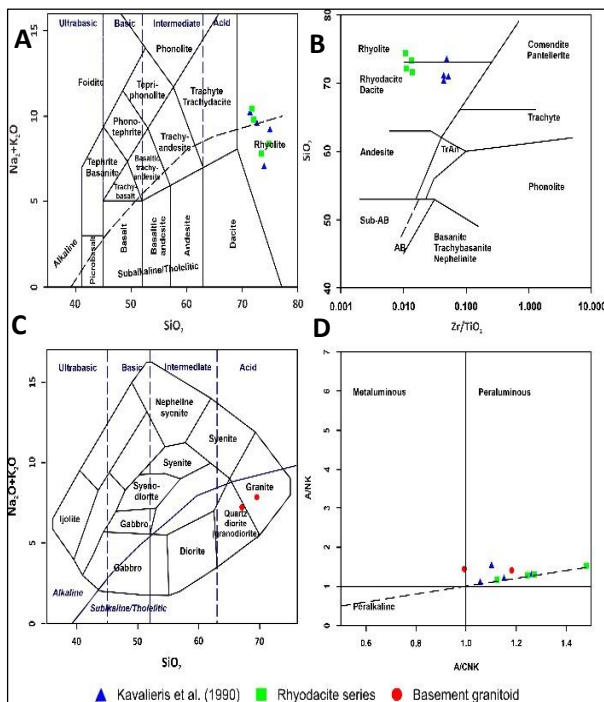


Fig. 7. (A) TAS diagram of Le Bas et al. (1986) that showing majority of the rhyodacite samples are grouped into rhyolite field; (B) Plot of immobile element ratios (Zr/TiO_2 vs Nb/Y) using Winchester and Floyd diagram (1977) has shown that all the rhyodacite samples were grouped into rhyolite to dacite/rhyodacite fields; (C) TAS diagram of Cox et al. (1979) that showing 2 sample granitoid basement from ILP-08 and ILP-10 are plot into granite and quartz diorite field; (D) $\text{A}/\text{CNK} - \text{A}/\text{NK}$ diagram from Shand (1943) for Iloa Nanasi samples that showing majority of sample is peraluminous granite.

When using the Winchester and Floyd (1977) plot of immobile element ratios (Zr/TiO_2 vs Nb/Y) as presented Fig 7B, the results are relatively consistent where rhyodacite samples from Iloa Nanasi mainly plot into the rhyolite to dacite/rhyodacite field. Meanwhile 2 samples of ILP-08 and ILP-10 are using TAS diagram of Cox et al. (1979) for plutonic rock has plot into granite and quartz diorite (granodiorite) fields (Fig 7C). Furthermore, the plot of $\text{A}/\text{CNK} - \text{A}/\text{NK}$ (Shand, 1943) majority of the samples grouped into peraluminous series, and only one sample from ILP-08 plot in transition to metaluminous series field (Fig 7D).

The trend of SiO_2 versus TiO_2 , P_2O_5 , Na_2O , MgO , FeO , and $\text{Fe}_2\text{O}_{3\text{total}}$ for all samples shows a depleted trend with increasing of SiO_2 (Fig 8A-F), where all the samples from the basement e.g., ILP-08 and ILP-10 have the lowest SiO_2 and highest TiO_2 , P_2O_5 , FeO , $\text{Fe}_2\text{O}_{3\text{total}}$, and MgO values compared to the sample taken from the rhyodacite dome complex e.g., ILP-01, ILP-03, ILP-04, and ILP-05. The samples have LOI values between 0.84 – 2.77 indicating occurrences of minor amounts of hydrous minerals probably due to alteration. In addition, by using primitive mantle plot (Sun and McDonough, 1989), the studied samples are consistent with the historical result where relatively enriched in LILE such as Rb, Ba, Th, U but depleted in HFSE e.g., Zr, Nb, Ta, and Ti (Fig. 9).

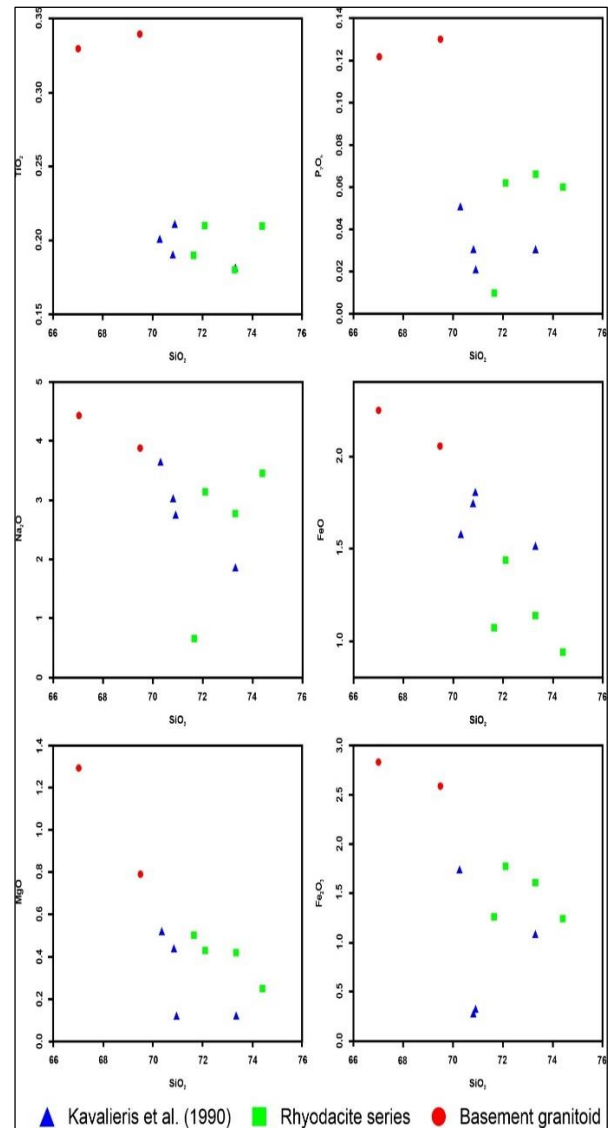


Fig. 8. Binary plot of Harker-type diagram for TiO_2 , P_2O_5 , Na_2O , MgO , FeO , and $\text{Fe}_2\text{O}_{3\text{total}}$ for all samples showing a depleted trend with increasing of SiO_2

Table 1. Geochemical data of Gn Pani sample from Iloa Nanasi and Kavalieris et al. (1990)

Sample Number, Drill Hole, and Depth	ILP-01 ILD278, 210m	ILP-03 NND094, 33.70m	ILP-04 ILD022, 116.50m	ILP-05 PCD04, 60m	ILP-08 LPD001, 125.50m	ILP-10 LPD003, 195m
Whole Rock (wt%)	Riodasit Porfiri	Riodasit Porfiri	Riodasit Ekuigranular	Riodasit Muda	Granodiorit	Granodiorit
Al ₂ O ₃	13.97	14.22	15.23	14.83	14.71	14.98
CaO	0.15	0.16	0.18	0.01	2.48	1.07
Cr ₂ O ₃	0.04	0.03	0.02	0.01	0.03	0.03
Fe ₂ O ₃	1.24	1.78	1.61	1.26	2.84	2.59
FeO	0.94	1.44	1.14	1.07	2.25	2.06
K ₂ O	4.87	6.65	4.99	9.75	2.78	4.00
MgO	0.25	0.43	0.42	0.50	1.29	0.79
MnO	<0.01	0.03	0.04	0.03	0.14	0.24
Na ₂ O	3.46	3.14	2.77	0.66	4.43	3.88
P ₂ O ₅	0.060	0.062	0.066	0.010	0.122	0.130
SiO ₂	74.39	72.09	73.31	71.63	67.03	69.49
TiO ₂	0.21	0.21	0.18	0.19	0.33	0.34
S	0.193	0.085	0.030	0.003	0.589	0.469
Total	99.7	99.5	100.0	99.7	99.5	99.5
LOI	0.89	0.64	1.41	0.84	2.77	1.45
FeO ^T	2.05	3.04	2.59	2.20	4.81	4.39
A/CNK	1.65	1.43	1.92	1.42	1.52	1.67
A/NK	1.68	1.45	1.96	1.42	2.04	1.90
Trace Elements (ppm)						
Al	68900	69800	67100	73800	73600	73600
Ca	1370	1470	1450	630	17800	7520
Cr	246	182	88	69	129	124
Cu	3	2	4	2	14	20
Fe (%)	0.73	1.12	0.89	0.83	1.75	1.6
K	38200	51700	34800	72000	22200	31000
Mg	1430	2400	2150	2880	7340	4490
Mn	57	218	209	152	953	1550
Na	23900	21500	17000	4690	31400	26800
Ni	5	5	3	3	9	11
P	250	260	250	50	490	530
S	1850	780	270	<50	6240	4420
Sc	3	3	2	3	4	4
Ti	1100	1070	1000	1040	1540	1710
V	16	16	14	15	37	36
Zn	49	41	50	47	462	102
Ag	0.6	0.9	0.1	<0.1	0.6	2.7
As	18	21	7	16	5	6
Ba	622	726	630	720	640	680
Be	2.7	3.1	3.5	3.1	1.9	2
Bi	0.31	0.46	0.31	0.36	1.24	4.25
Cd	0.29	0.06	<0.05	<0.05	5.08	0.69
Co	3	2	1	2	5	5
Cs	4.3	5.1	11.1	25.2	3.7	4.2
Ga	14.3	15.3	15.2	17.1	18.7	19.6
Ge	1.4	1.4	1.5	2	1.5	1.4
Hf	1.1	1.1	1.1	1.4	0.2	0.2
In	<0.05	<0.05	<0.05	<0.05	0.08	0.05
Li	18.7	20.8	22.9	33.8	13.4	12.5
Mo	1	0.9	0.3	0.3	4.4	37
Nb	9	8.9	11.6	11.2	6.3	7
Pb	54	61	51	44	79	394
Rb	215	269	223	674	111	165
Re	<0.05	<0.05	<0.05	<0.05	<0.05	<0.05
Sb	6.5	3.4	3.4	20.3	0.7	1.7
Se	<1	<1	<1	<1	<1	<1
Sn	1.6	1.9	2	2.5	1.8	2.3
Sr	359	485	223	123	443	447
Ta	1.37	1.39	1.61	1.8	0.72	0.76
Te	<0.1	<0.1	<0.1	<0.1	0.2	0.5
Th	8.2	9.46	10.6	11.6	7.99	9.42
Tl	3.1	3.97	2.29	8.48	0.94	1.62
U	3.82	4.85	6.04	6.12	1.81	2.3
W	6.7	4.6	1.6	3.4	6.9	11.1
Y	9	13.7	13.9	14.5	12.9	12.7
Zr	22.6	22.8	23.8	26	2.4	2.9
Ce	28.8	38.9	38.9	34.1	52	56.6
Dy	1.5	2	2.3	2.2	2.3	2.4
Er	0.9	1.2	1.3	1.4	1.2	1.2
Eu	0.4	0.6	0.5	0.5	0.7	0.8
Gd	2	2.6	2.4	2.6	3.3	3.4
Ho	0.3	0.4	0.4	0.4	0.4	0.4
La	13.9	18.9	18.2	17.5	25.4	27.2
Lu	0.16	0.19	0.22	0.24	0.15	0.16
Nd	12.1	15	13.7	13.6	20.2	21.1
Pr	3.16	4	3.72	3.66	5.23	5.63
Sm	2.4	2.9	2.6	2.8	3.8	4
Tb	0.25	0.32	0.31	0.34	0.39	0.39
Tm	0.1	0.2	0.2	0.2	0.2	0.2
Yb	1	1.3	1.2	1.5	1	1.1

* Data from Kavalieris et al. (1990); ** this study

The higher anomalous of K-Pb-Sr in Iloa Nanasi sample also similar to the studied sample in north arm Sulawesi was reported by Elburg and Foden (1998).

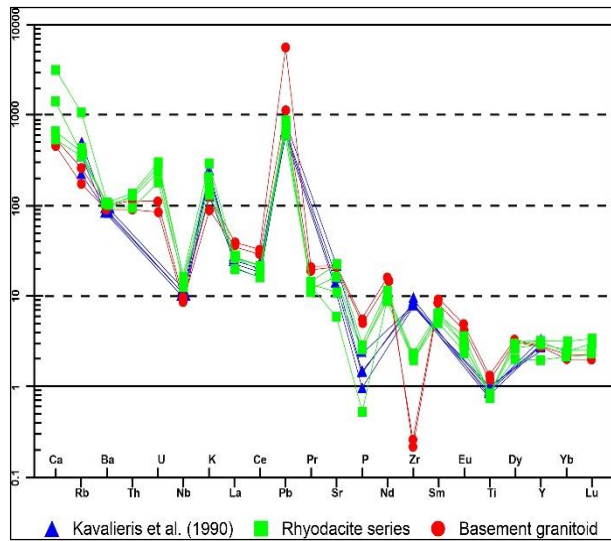


Fig. 9. Normalised primitive mantle plot for studied sample and historical data from Kavalieris et al. (1990) showing relatively enriched in LILE such as Rb, Ba, Th, U but depleted in HFSE e.g., Zr, Nb, Ta, and Ti. Positive anomalous of K-Pb-Sr in Iloa Nanasi sample also similar to the studied sample in north arm Sulawesi was reported by Elburg and Foden (1998).

5. Discussion

Iloa Nanasi gold deposit is hosted in rhyodacite that is interpreted as part of Pliocene sub-aerial volcanism and formed eroded volcanic center about 3.5 km in diameter (Trail et al., 1974; Carlile et al., 1990; Kavalieris et al., 1990). Kavalieris et al. (1990) sample, suggested that major and trace elements compositions are related to gold mineralisation, which has been indicated by fractional crystallization at depth following the differentiation magma chamber beneath the Pani dome complex.

In this study, we combined the analytical result of petrography and whole-rock geochemistry to assess the petrogenetic association of all samples. A total of 10 samples taken from rhyodacite dome were plotted into the TAS diagram for volcanic rock provided by Le Bas et al. (1986) and using Winchester and Floyd diagram (1977) for immobile element ratio of (Zr/TiO₂ versus Nb/Y) have shown that all the rhyodacite samples were grouped into rhyolite to dacite/rhyodacite fields (Fig 7A-B). The petrography observation of 4 studied samples shows ILP-01 and ILP-03 having more porphyritic textures with up to 60% of volume, while in samples ILP-04 and ILP-05 are less than 25% of volume. The result of analysis also shows slightly depleted K₂O in samples ILP-01, ILP-03, and ILP-04 (range from compared to ILP-05. This result could be correlated to the destruction of K-bearing mineral, e.g., potassium feldspar in rhyodacite during alteration. In contrast, the elevated K₂O in ILP-05 is correlated to the preservation as the sample part of late intrusion phase that is not hosting mineralization in Iloa Nanasi.

Two granitoid samples examined from Lone Pine e.g., ILP-08 and ILP-10 are subdivided into alkali feldspar granite based on petrography. The granitoid examined are phaneritic, equigranular textural composition, hypidiomorphic, interlocking, and dominant subhedral crystal composition range from 50 μm to 3 mm size consisting of quartz, K-feldspar, plagioclase, biotite, hornblende with some accessories mineral e.g., apatite and tourmaline. The results of whole rock

geochemistry presented in Fig 7C range from quartz diorite to granite composition when plot into TAS diagram (SiO₂ vs Na₂O + K₂O) provided by Cox et al. (1979).

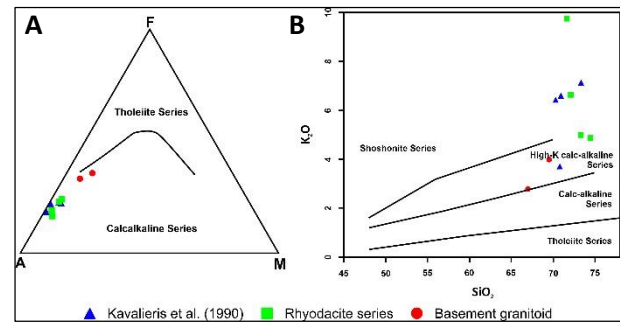


Fig. 10. (A) Magma series of Iloa Nanasi samples from AFM diagram (Irvine and Baragar, 1971) shows most of samples in calc-alkaline series. (B) The plot from Peccerillo and Taylor (1976) showing to High-K calc-alkaline series.

The petrogenetic association of all samples from Iloa Nanasi is using the AFM diagram (Irvine and Baragar, 1971) to distinguish the magma series field, showing sample trends in calc-alkaline series (Fig 10A). The calc-alkaline samples from Iloa Nanasi also can be grouped in the peraluminous by their high ANK ratio (1.39 – 2.05) and ACNK/ASI ratio (1.37 – 1.92) refer to the classification given by Shand (1943) and Frost et al. (2001) as shown in Fig 7D. Meanwhile, when plotted into SiO₂ – K₂O of Peccerillo and Taylor (1976) shows two trending result: (a) Granitoid sample, which represents the older basement unit, falls into the high-K calc-alkaline series that indicates more potassic composition, and (b) Rhyodacite samples lied from high-K calc-alkaline to the shoshonite series (Fig 10B).

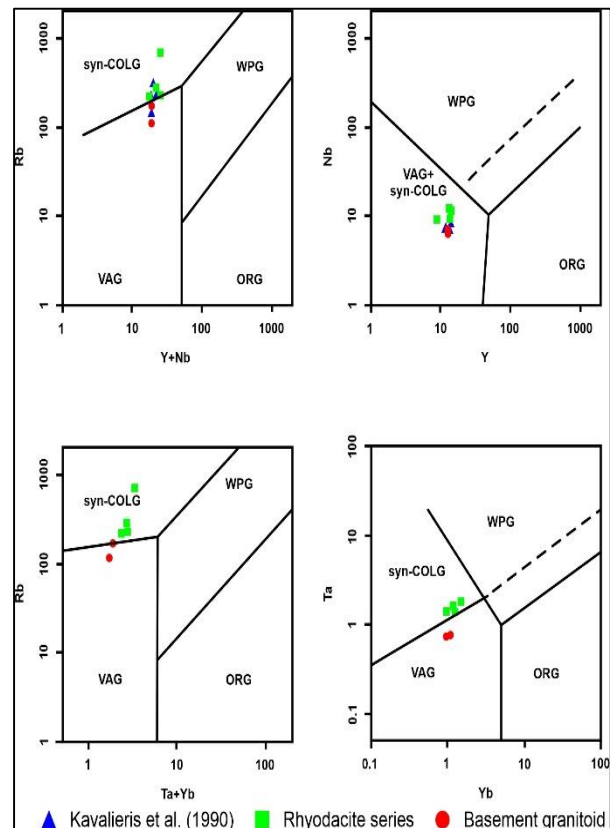


Fig. 11. Granite tectonic discriminant from Pearce et al. (1984) for samples in Iloa Nanasi

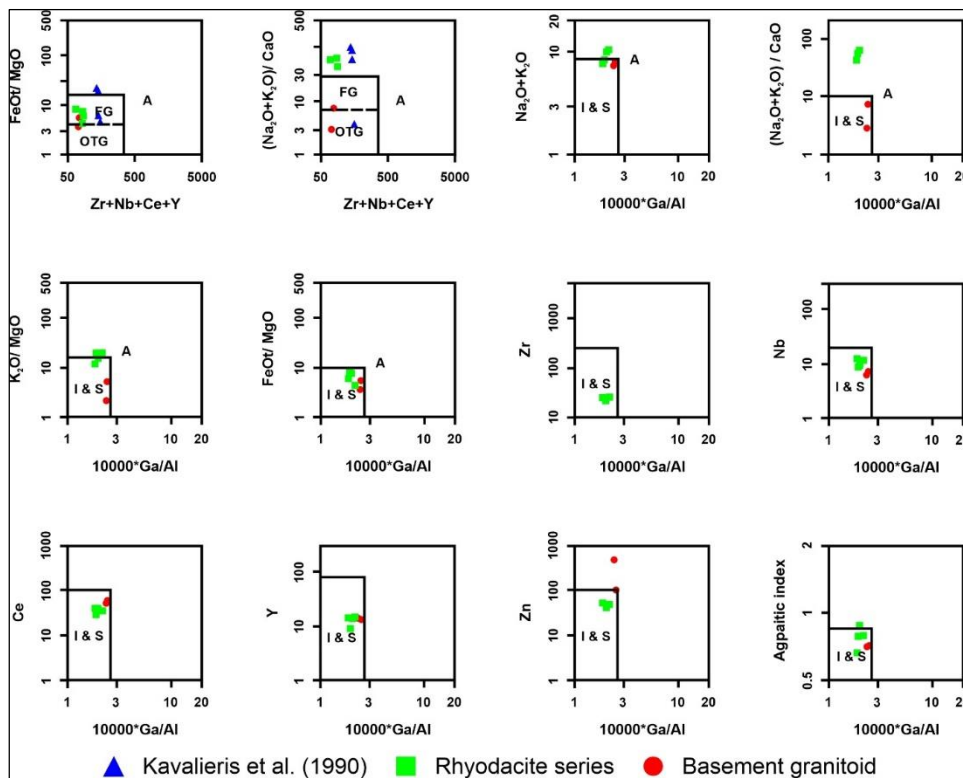


Fig. 12. Granite tectonic discriminant from Pearce et al. (1984) for samples in Ilota Nanasi

The occurrences of shoshonitic magma associated with the high-K calc-alkaline magma in Sulawesi also has been reported by Priadi et al. (1994), Elburg and Foden (1998), Elburg et al. (2003), Hennig et al. (2015), Maulana et al. (2016). The changing of magma series from calc-alkaline to shoshonitic affinity could be correlated to the variation in pressure of fractionation of parental magma as proposed by Meen (1987). The changing of pressure could be occurred in a subduction or post-subduction related environments where the magma can be derived from the melting of mantle material after the mantle or lower crustal was metasomatised during a former episode of subduction (Priadi et al., 1994; Beccaluva et al., 2013; Couzinie et al., 2016; Maulana et al., 2016; Im et al., 2021; Glaser et al., 2022).

The trace elements binary plot of Rb-Y-Nb and Rb-Yb-Ta from Ilota Nanasi sample can be used for the identification of tectonic settings proposed by Pearce et al. (1984) which suggests four main groups based on their plutonic setting. According to the result of the element binary diagram presented in Fig 11, most samples fall into the syn-COLG and VAG field that associated with collision and volcanic arc origin. Whalen et al. (1987) plot of samples in Fig 12 suggested the I- and S-type granite for Ilota Nanasi samples that derived from source of igneous rocks and/or from the partial melting of metasedimentary source rocks. The spider plot of MORB-normalised in Fig 8 provides values of Nb that are generally higher than Zr suggesting the origin of either a continental arc or a collisional signature (Pearce and Peate, 1995; Elburg and Foden, 1999, Elburg et al., 2003). The spider diagram demonstrates strong positive Pb anomalies that correlated to subduction related as reported by Elburg et al. (2003).

6. Conclusion

The geochemistry data of rhyodacite and granitoid rocks in Ilota Nanasi has shown the changing of composition over time. The older unit was typically associated with high-K calc alkaline series and then evolved to shoshonite series for the younger unit. The changing of magma series is considered as

product of crystallization differentiation of evolved parental magma or derived from the melting of mantle material after the mantle or lower crustal was metasomatised during a former episode of subduction. This result is also supported from the trace element binary plot that suggests tectonic setting associated with the collision, volcanic arc origin and/or subduction-related tectonic setting.

Acknowledgement

This paper report is selected results from a MSc thesis completed at the Geological Engineering of the University of Padjadjaran, Indonesia by first author. Authors would like to thank the management of J Resources Nusantara for providing support, access to the exploration data, and samples during research and permission to publish this paper. The expressions of gratitude are given to Agus Irfan, Arief Iman Santosa, Arif Eko Prihandoyo, Atmasari Rura, Muh Taufik, Widji Pramadjati, Yunus Nakka, Koppe, Buyung, Mario Eko Cipta Lubis, Stephanus Ivan Lette, Dini Pertiwi, Lingkan Sherlyn Sibirian, Muh Faqih Alfyan, and Ryan Djodi Pratama for their support in the fieldwork and during data collection and construction of the paper, and special thanks to Raden Aditya Suryadharna and Ferdiansyah for preparing the figures. This research benefited from interaction with the geological team in the Greenfield Exploration Department of PT J Resources Nusantara and PT Gorontalo Sejahtera Mining during 2016 – 2020.

References

- Apandi, T., and Bachri, S., 1997. Geological map of the Kotamobagu sheet, Sulawesi. Geological Research and Development Centre, 1 p.
- Bachri, S., Sukido, and Ratman, N., 1993. Geological map of the Tilamuta sheet, Sulawesi. Geological Research and Development Centre, 1 p.
- Basuki, A., Sumanagara, A.D., and Sinambela, D., 1994. The Gunung Pongkor gold-silver deposit, West Java, Indonesia. *J. Geochem. Explor.* 50, 371 - 391

- Beccaluva, L., Bianchini, G., Mameli, P., Natali, C., 2013. Miocene shoshonite volcanism in Sardinia: Implications for magma sources and geodynamic evolution of the central-western Mediterranean. *Lithos* 180, 128–137
- Carlile, J.C., Digdowirogo, S., and Darius, K., 1990. Geological setting, characteristics and regional exploration for gold in the volcanic arcs of North Sulawesi, Indonesia. *Journal of Geochemical Exploration*, Vol. 35, pp. 105 – 140.
- Clark, L.V., and Gemmell, J.B., 2018. Vein stratigraphy, mineralogy, and metal zonation of the Kencana low-sulfidation epithermal Au-Ag deposit, Gosowong goldfield, Halmahera Island, Indonesia. *Economic Geology*, Vol 113, 209 - 236.
- Cox, K.G., Bell, J.D., and Pankhurst, R.J., 1979. The interpretation of igneous rock. George Allen and Unwin, London.
- Couzinié, S., Laurent, O., Moyen, J.-F., Zeh, A., Bouilhol, P., Villaros, A., 2016. Post-collisional magmatism: crustal growth not identified by zircon Hf-O isotopes. *Earth Planet. Sci. Lett.* 456, 182–195
- Effendi, A.C., and Bawono, S.S., 1997. Geological map of the Manado sheet. Geological Research and Development Centre, 1 p.
- Elburg, M., and Foden, J., 1998. Temporal changes in arc magma geochemistry, northern Sulawesi, Indonesia. *Earth and Planetary Science Letters* 163, 381 – 398.
- Elburg, M., and Foden, J., 1999. Source for magmatism in Central Sulawesi: Geochemical and Sr-Nd-Pb constraints. *Chemical Geology* 156, 67 – 93.
- Elburg, M., Van Leeuwen, T.M., Foden, J., and Muhandjo, 2003. Spatial and temporal isotopic domains of contrasting igneous suites in Western and Northern Sulawesi, Indonesia. *Chemical Geology* 199, 243 – 276.
- Frost, B.R., Barnes, C.G., Collins, W.J., Arculus, R.J., Ellis, D.J., and Frost, C.D., 2001. A geochemical classification for granitic rocks. *Journal of Petrology*, Vol. 42, 2033 – 2048.
- Glaser, L., Grosche, A., Voudouris, P.C., and Haase, K.M., 2022. The high-K calc-alkaline to shoshonitic volcanism of Limnos, Greece: implications for the geodynamic evolution of the northern Aegean. *Contributions to Mineralogy and Petrology*, 177: 73.
- Hall, R., 2002. Cenozoic geological and plate tectonic evolution of SE Asia and the SW Pacific: Computer based reconstructions, model and animations. *Journal of Asian Earth Sciences*, Vol. 20, 353 – 434.
- Hamilton, W., 1979. Tectonics of the Indonesian region. U.S. Geological Survey, Professional Paper, p. 1078, 345.
- Hennig, J., Hall, R., Armstrong, R.A., 2015. U-Pb zircon geochronology of rocks from west Central Sulawesi, Indonesia: extension-related metamorphism and magmatism during the early stages of mountain building. *Gondwana Res.*
- Im, S., Park, J.W., Kim, J., Choi, S.G., and Lee, M.J., 2021. Petrogenesis of coeval shoshonitic and high-K calc-alkaline igneous suites in the Eopyeong granitoids, Taebaeksan Basin, South Korea: Lithospheric thinning-related Early Cretaceous magmatism in the Korean Peninsula. *Lithos*: 392 - 393
- Irvine, T.N., and Baragar, W.R.A., 1971. A guide to the chemical classification of the common volcanic rocks. *Canadian Journal of Earth Sciences*, 8, 523 – 548.
- Kadariusman, A., 2011. Basement rocks of Sulawesi and their contribution to the metallogenic formation. Proceedings of the Sulawesi Mineral Resources Seminar 2011, Manado, North Sulawesi
- Katili, J.A., 1978. Past and present geotectonic position of Sulawesi. *Tectonophysics* 45, 289 – 322.
- Kavalieries, I., Nowak, D., Digdowirogo, S., and Darius, K., 1982. Geological report on the Gunung Pani gold prospect, NE Sulawesi (rep), PT Tropic Endeavor Indonesia, 94p.
- Kavalieries, I., Walshe, J.L., Halley, S., and Harrold, B.P., 1990. Dome-related gold mineralisation in the Pani Volcanic Complex, North Sulawesi, Indonesia: A study of geologic relations, fluid inclusions, and chlorite compositions. *Economic Geology* Vol. 85, pp. 1208 – 1225.
- Kavalieries, I., van Leeuwen, T.M., and Wilson, M., 1992. Geological setting and styles of the mineralisation, north arm of Sulawesi, Indonesia. *Journal of Southeast Asian Earth Sciences*, Vol. 7, pp. 112 – 129.
- Koperberg, M., 1929. *Bouwstoffen voor de geologie van de Residentie Menado, Jaarboek Mijnwezen Nederlands Indië* (57) 2: 1 – 446.
- Le Bas, M.J., Le Maitre, R.W., Streckeisen, A., and Zanettin, B., 1986. A chemical classification of volcanic rocks based on the total alkali-silica diagram. *Journal of Petrology*, 27, 745-750.
- Maulana, A., Watanabe, K., and Yonezu, K., 2013. Origin of magnetite- and ilmenite-series granitic rocks in Sulawesi, Indonesia: magma genesis and regional metallogenic constraint. *Procedia Earth and Planetary Sciences*, Vol. 6, 50 – 57.
- Maulana, A., Imai, A., van Leeuwen, T.M., Watanabe, K., Yonezu, K., Nakano, T., Boyce, A., page, L., and Schersten, A., 2016. Origin and geodynamics setting of the Late Cenozoic granitoids in Sulawesi, Indonesia. *Journal of Asian Earth Sciences*, Vol. 124, pp. 102 – 125.
- Maulana, A., Christy, A.G., Ellis, D.J., and Brocker, M., 2019. The distinctive tectonic and metamorphic history of the Barru Block, South Sulawesi, Indonesia: Petrological, geochemical and geochronological evidence. *Journal of Asian Earth Science*, Vol. 172, pp. 170 – 189.
- Marjoribanks, R., 1998. The geology and mineralisation of the Pani Volcanic Complex, North Sulawesi: An air photo interpretation (rep), PT Newcrest Nusa Sulawesi, 22 p.
- Meen, J.K., 1987. Formation of shoshonites from calc-alkaline basalt magmas: geochemical and experimental constraints from the type locality. *Contributions to Mineralogy and Petrology*, Vol 97, 333 - 351.
- McConnochie, M.R., 1999. Exploration of the Pani epithermal gold district, Northern Sulawesi, Indonesia (rep), PT Newcrest Nusa Sulawesi, 70 p.
- McLellan, G.A., Bird, M.C., and Pertsell, B.A., 1975. Progress report Gunung Pani gold prospect and associated regional exploration Block 2, Sulawesi, Indonesia (rep), PT Tropic Endeavor Indonesia, 109 p.
- Pearce, J.A., Harris, N.B.W., and Tindle, A.G., 1984. Trace element discrimination diagrams for the tectonic interpretation of granitic rocks. *Journal of Petrology*, Vol 25, 956 – 983.
- Pearce, J.A., and Peate, D.W., 1995. Tectonic implications of the composition of volcanic arc magmas. *Annu. Rev. Earth Planet. Sci.* 23, 251 – 285.
- Pearson, D.F., and Caira, N.M., 1999. Geology and metallogeny of central north Sulawesi. Pacrim'99 Congress, Australian Institute of Mining and Metallurgy 4/99, 311 – 326
- Peccerillo, A., and Taylor, S.R., 1976. Geochemistry of the Eocene calc-alkaline volcanic rocks in the Kastamonu area, northern Turkey. *Contrib Miner Petrol* 58:63–81
- Pratama, B., and Wijayadi, D., 2019. Mineral Resources Estimate for Iloa Nanasi – Pani Gold Project Prepared for PT. Gorontalo Sejahtera Mining (rep), Cube

- Consulting Pty Ltd.
- Priadi, B., Polve, M., Maury, R.C., Bellon, H., Soeria-Atmaja, R., Joron, J.L., and Cotton, J., 1994. Tertiary and Quaternary magmatism in Central Sulawesi: chronological and petrological constraints. *Journal of Southeast Asian Earth Sciences*, Vol. 9, 81 – 93.
- Priadi, B., 2011. Sulawesi magmatic arcs. *Proceedings of the Sulawesi Mineral Resources 2011, MGEI Annual Convention, Manado, North Sulawesi*, pp. 111 – 120.
- Ratman, N., 1976. Geologic map of the Tolitoli quadrangle, North Sulawesi: Indonesia, scale 1 : 250.000. Geological Survey of Indonesia, 1p.
- Rompo, I., and Santoso, B.S.T.J., 2019. Laporan eksplorasi proyek tambang emas Pani tahun penyelidikan 2011 – 2018 (rep), PT J Resources Nusantara, 411 p.
- Rura, A., and Siburian, L.S., 2019. Pani ASD clay domain study (rep), PT J Resources Nusantara, 15 p.
- Shand, S.J., 1943. *The eruptive rocks*, 2nd edition. New York: John Wiley, 444p.
- Silver, E.A., McCaffrey, R., Joyodiwiryo, Y., and Stevens, S., 1983. Ophiolite emplacement by collision between the Sula platform and the Sulawesi Island arc, Indonesia. *Journal of Geophysical Research*, Vol. 88, pp. 9419 – 9435.
- Stock, D., 2013. Pani 2013 resources update (rep), internal memo of PT J Resources Nusantara, 9 p.
- Sukanto, R., 1973. Reconnaissance geological map of Palu area, Central Sulawesi, scale 1 : 250.000. Geological Survey of Indonesia, 1 p.
- Sun, S.-s., and McDonough, W.F., 1989. Chemical and isotopic systematics of oceanic basalts: implications for mantle composition and processes. In: Saunders, A.D., Norry, M.J. (Eds.), *Magmatism in the Ocean Basins*. Geological Society Special Publication, pp. 313 – 345
- Szentpeteri, K., 2017. Pani, 19 metallurgical samples and petrography results, a brief summary (rep), PT J Resources Nusantara, 14 p.
- Szentpeteri, K., 2019. Pani geometallurgy – gold characterization and deportment study (rep), PT J Resources Nusantara, 23 p.
- Trail, D. S., John, T. V., Bird, M. C., Obial, R. C., Petzel, B. A., Abiong, D. B., Parwoto, and Sabagio, 1974. The general geological survey of Block 2, Sulawesi Utara, Indonesia (rep), PT Tropic Endeavour Indonesia, 68 p.
- Van Leeuwen, T.M., and Pieters, P.E., 2011. Mineral deposits of Sulawesi. *Proceedings of the Sulawesi Mineral Resources, MGEI Annual Convention, Manado, North Sulawesi*, 131 p.
- Van Schelle, C.J., 1889. Verslag van een onderzoek naar de waarde van bekende goudvindplaatsen in de afdeling Gorontalo. *Jaarboek van het Mijnwezen*, pp. 39 - 55.
- Verdiansyah, O., 2023. Hasil analisis petrografi 6 sampel Gn. Pani, Gorontalo (rep), PT Geomineral Sukma Analisis, 43p.
- Whalen, J.B., Currie, K.L., and Chappell, B.W., 1987. A-type granites: geochemical characteristics, discrimination, and petrogenesis. *Contributions to Mineralogy and Petrology*, Vol. 95, 407 – 418.
- Whittle, A.W.G., 1975. Report Misc/130 Silicified volcanics, Sulawesi Block 2 (rep), Endeavour Oil Company N/L, 32p.
- Winchester, J.A., and Floyd, P.A., 1977. Geochemical discrimination of different magma series and their differentiation product using immobile elements. *Chemical Geology*, 20, 325-343.
- Zhang, X., Tien, C.Y., Chung, S.L., Maulana, A., Mawaleda, M., Chu, M.F., Lee, H.Y., 2020. A Late Miocene magmatic flare-up in the West Sulawesi triggered by Banda slab rollback. *Geological Society of America*, Vol. 132, pp. 2517 – 2528.



© 2023 Journal of Geoscience, Engineering, Environment and Technology. All rights reserved. This is an open access article distributed under the terms of the CC BY-SA License (<http://creativecommons.org/licenses/by-sa/4.0/>).